

Accepted Manuscript

Site preference for luminescent activator ions in doped fluoroperovskite RbZnF₃

Sanjay Kumar Saroj, Rajamani Nagarajan



PII: S1386-1425(18)30418-9
DOI: doi:[10.1016/j.saa.2018.05.028](https://doi.org/10.1016/j.saa.2018.05.028)
Reference: SAA 16051

To appear in: *Spectrochimica Acta Part A: Molecular and Biomolecular Spectroscopy*

Received date: 12 March 2018
Revised date: 5 May 2018
Accepted date: 8 May 2018

Please cite this article as: Sanjay Kumar Saroj, Rajamani Nagarajan , Site preference for luminescent activator ions in doped fluoroperovskite RbZnF₃. The address for the corresponding author was captured as affiliation for all authors. Please check if appropriate. Saa(2017), doi:[10.1016/j.saa.2018.05.028](https://doi.org/10.1016/j.saa.2018.05.028)

This is a PDF file of an unedited manuscript that has been accepted for publication. As a service to our customers we are providing this early version of the manuscript. The manuscript will undergo copyediting, typesetting, and review of the resulting proof before it is published in its final form. Please note that during the production process errors may be discovered which could affect the content, and all legal disclaimers that apply to the journal pertain.

Site preference for luminescent activator ions in doped fluoroperovskite RbZnF₃

Sanjay Kumar Saroj and Rajamani Nagarajan*

Materials Chemistry Group, Department of Chemistry, University of Delhi,

Delhi 110 007 INDIA

Mr. Sanjay Kumar Saroj (sarojsk1989@gmail.com)

Professor Rajamani Nagarajan (rnagarajan@chemistry.du.ac.in) * Corresponding Author

ORCID: 0000-0002-0983-7814

ACCEPTED MANUSCRIPT

Abstract

With the dual objective of investigating the site preferences of larger sized activator ions and to append luminescence property to the perovskite structured RbZnF_3 , doping of manganese(II), cerium(III), europium(III) and terbium(III) ions (5 mol %) was carried out. Although cubic symmetry of RbZnF_3 was preserved for all the doped samples, site preference of rare-earth ions for the A-site Rb^+ leading to an inverse perovskite arrangement has been noticed from careful analysis of lattice parameters from refinement of powder X-ray diffraction data. Undoped RbZnF_3 exhibited rod-like morphology in the transmission electron microscopic image. In addition to an intense band around 230 nm assignable to the charge transfer from ZnF_3^- to Rb^+ , typical transitions of respective dopant ions were observed in their UV-visible spectra. The doped samples showed luminescence in blue, green and red regions and time decay experiments suggested the uniform dispersion of them without any clustering effect. The lower phonon energy of RbZnF_3 matrix by virtue of the presence of heavier rubidium at the A-site together with its doping with rare-earth ions resulting in an inverse perovskite like arrangement could favour their utility in various practical applications.

Keywords: Fluoroperovskites; Wet-chemical synthesis; X-ray diffraction; Luminescence; Inverse perovskite.

Introduction

The compositional flexibility along with wide occurrence of the perovskite structure adorns them with many interesting useful applications and thus attracted the attention of scientists of various disciplines [1-3]. Of these, their role as hosts for holding luminescent ions has been investigated at length [4, 5]. Though this structure is exhibited by a variety of compounds such as oxides, fluorides and chlorides, mixed metal fluorides are preferred host for holding luminescent ions as they are insulating and exhibit low phonon energy [6-8]. In an ideal cubic perovskite with the formula AMF_3 , 'A' is the monovalent atom (K, Rb, and Cs) and 'M' is the divalent atom (Mg, Mn, Co, Ni, Zn and Ca). Following the widely accepted tolerance factor based on the ionic radii of A^+ , M^{2+} and F, the perovskite structure was found to be stable with a tolerance factor in the range of 0.8-1.0. This limit has been further extended to 0.707-1.225 [1]. For the tolerance factor in the range 0.707-1.0, distortion of ideal perovskite structure was observed primarily due to the tilting of MF_6 octahedra, while shifting of M^{2+} ions away from the center of MF_6 octahedra has been found to result in distortion for compounds with tolerance factor between 1.0 and 1.225 [9]. The divalent transition metal ions of the first row from Mn^{2+} to Zn^{2+} with the alkali metal ion show interesting variations when crystallize in perovskite structure which receive contributions from both the size of the alkali metal ions as well as from the electronic structure of the transition metal ions [10]. Considering the $RbMF_3$ family, cubic perovskite without distortion has been observed for $M = Mn^{2+}$, Co^{2+} and Zn^{2+} , whereas tetragonal and hexagonal distortion was exhibited by $RbCuF_3$ and $RbNiF_3$, respectively [11, 12]. The hexagonal modification has been induced in other systems either by temperature or by substituting with appropriate M^{2+} ions [13, 14]. Transformation from hexagonal to cubic in $RbNiF_3$ has been found to be induced by applying physical pressures [15]. In some cases, even co-doping with alkali metal and rare earth

ion has given rise to the hexagonal perovskite arrangement [16]. Although most of the studies have been carried out by growing single crystals [16, 17], solution based and bulk synthesis have not been explored to a greater extent given the scenario of the recent discovery of interesting solar cell applications in hybrid perovskite system [18, 19]. Another important aspect with respect to mixed metal fluorides from the luminescence property perspective is their low phonon energy as compared to their oxide counterparts. Among mixed metal fluorides, reduction in phonon energy and decrease in multiphonon relaxation have been known to occur for alkali metals in the order $\text{Li} > \text{Na} > \text{K} > \text{Rb}$ [20-26]. Therefore, it will be a natural consequence to evaluate the Rb-containing perovskites as host matrix to achieve maximum efficiency. Also, such an exercise will reveal the effect of chemical pressure on the overall symmetry of the perovskite lattice as well as the local site preferences for dopant ions. The presence of divalent zinc ion at the B-site in ABF_3 would impart transparency to the host matrix due to its d^{10} electronic configuration. Generally, aqueous medium for solution based synthesis of mixed metal fluorides has the drawback of hydrolysis effect resulting in the deterioration of photoluminescence intensity and lifetime. The hydrolysis effect can be minimized by conducting fluorination reactions in non-aqueous medium. If it can be achieved at room temperature, it can certainly reduce the concentration of defects at the lattice sites induced by high temperature reaction conditions. With this entire scientific background, current study has been undertaken to understand the effect of doping divalent (Mn^{2+}) and trivalent rare-earths (Ce^{3+} , Eu^{3+} and Tb^{3+}) on the structure and luminescence property of cubic RbZnF_3 .

Materials and methods

For the synthesis, zinc chloride salt was prepared in situ by reacting 0.0833 g (1 *mmol*) of ZnO (Sigma Aldrich 99.9%) with minimum amount of freshly prepared HCl (1:1 by volume). To this,

0.3135 g (3 *mmol*) of RbF (Alfa Aesar 99.9%) dissolved in 40 mL of methanol (Spectrochem) was added drop-wise under constant stirring. It was stirred for 4 h at room temperature to result in a white colored precipitate which was separated from the mother liquor by filtration. The filtrate was checked for the presence of Cl⁻ ions by adding aqueous AgNO₃ solution. The washing was continued till the filtrate did not yield a curdy-white precipitate. 0.0099 g (0.05 *mmol*) of MnCl₂.4H₂O (Alfa Aesar 99.9%), 0.0183 g (0.05 *mmol*) of EuCl₃.6H₂O (Sigma Aldrich 99.9%), 0.0186 g (0.05 *mmol*) of TbCl₃.6H₂O (Alfa Aesar 99.9%) and 0.0217 g (0.05 *mmol*) of Ce(NO₃)₃.6H₂O (Alfa Aesar 99.5%) were used along with ZnO, (0.0774 g, 0.95 *mmol*) and RbF (0.3135 g (3 *mmol*)) to synthesize doped samples following a similar procedure employed for making RbZnF₃.

Powder X-ray diffraction (PXRD) patterns of the samples were recorded using PANalytical X'Pert diffractometer, equipped with Xenon detector, employing CuK α radiation ($\lambda = 1.5418 \text{ \AA}$) with a scan rate of 1.0 s/step and step size of 0.02° at 25°C over 2 θ range of 20-70°. High resolution transmission electron microscopic (HR-TEM) images were recorded using a FEI Tecnai electron microscope operating at an accelerating voltage of 200 kV (Electron Optics). UV-visible diffuse reflectance spectra of the samples were recorded using Perkin-Elmer (Lambda-35) spectrometer attached with an integrating sphere. BaSO₄ was used as the reference. Reflectance data were converted to absorbance using Kubelka-Munk function. The conventional excitation and emission spectral measurements were carried out in powder form using Horiba Jobin Yvon Fluorolog modular spectrofluorometer at room temperature employing a continuous-wave xenon lamp source as well as Cary Eclipse Fluorescence Spectrophotometer G9800AA.

Results and discussion

The reaction between rubidium fluoride and zinc chloride (from ZnO) could be represented by the following equations:



Dense white color solid, from this reaction after the removal of RbCl, was subjected to X-diffraction experiments. In Fig. 1, PXRD pattern, EDX analysis, TEM, HR-TEM and selected area electron diffraction (SAED) pattern of the same have been presented. In the PXRD pattern, the position and intensity profile of the observed reflections matched with that of JCPDS File for RbZnF₃ (No. 20-1016) and confirmed the formation of cubic perovskite structure. The EDX spectrum of the sample confirmed the presence of Rb, Zn and F and equal concentrations of Rb and Zn. This was quite encouraging to be further applied for synthesizing doped samples. Rod-like morphology was observed in TEM image of the sample and this was quite similar to the morphology reported earlier for KZnF₃ obtained by solvothermal synthesis [27]. Lattice fringes with distances of 0.29 and 0.23 nm corresponding to (110) and (111) *hkl* planes of cubic structure were evident in HR-TEM analysis. Bright spots were observed in the SAED pattern indicative of crystalline nature of the sample. The spots were indexed corresponding to (110), (111), (200), (211) and (220) *hkl* planes of cubic RbZnF₃. All these confirmed bulk as well as microscopic purity of our sample.

✓ In order to determine the concentration of the dopant to be introduced in RbZnF₃, samples with two different concentrations (5 and 10 mol %) of Mn²⁺ were prepared. From the powder X-ray diffraction patterns of these samples, it was abundantly clear that dopant concentration of 5 mol % produced monophasic sample and phase separation occurred when it was increased to 10

mol % (Fig. 2(a) and Fig.S1). It was therefore decided to investigate 5 mol % of dopant concentration for other impurity ions, viz., Ce^{3+} , Eu^{3+} and Tb^{3+} -ions as it would facilitate to compare their spectral behavior. PXRD patterns of RbZnF_3 doped with 5 mol% of Ce^{3+} , Eu^{3+} and Tb^{3+} -ions have been presented in Fig. 2. In all these doped samples, peaks pertaining to cubic symmetry were present. While doping of Mn^{2+} for six-fold coordinated Zn^{2+} could be reasoned out primarily based on ionic radii of these two ions (Zn^{2+} :0.74 Å versus Mn^{2+} :0.83 Å). However, such a scenario did not prevail for the rare-earth ions as they possessed ionic radii way higher than Zn^{2+} -ion as well as exhibited preference for coordination numbers greater than six. When the divalent and trivalent ions could be interchanged between the tetrahedral and octahedral coordinated environments in a spinel arrangement, inverse spinel nomenclature was generally used. A similar situation prevailed in perovskite structure. In an inverse perovskite structural arrangement, ions with bigger size could occupy 12-fold coordinated position irrespective of their higher valence. Higher probability of such a scenario was feasible in fluoroperovskites [28]. Considering therefore higher probability of the doped RE^{3+} -ions for Rb^+ in RbZnF_3 , Rietveld refinement of PXRD patterns of RE^{3+} doped samples were performed considering them to replace XII coordinated Rb^+ -ion in perovskite structure (Fig. 2). For the Mn^{2+} doped samples, Rietveld refinement of PXRD pattern was carried out by including Mn^{2+} in place of six coordinated Zn^{2+} in the perovskite structural arrangement (Fig. 2). The crystallographic details from the Rietveld refinements of PXRD patterns and the atomic parameters after the final cycle of refinement have been compiled in Table 1-3. The refined parameter for cubic RbZnF_3 and 5 mol% Mn^{2+} , Tb^{3+} , Eu^{3+} and Ce^{3+} doped samples were 4.1190 (16), 4.1238 (28), 4.1141 (09), 4.1158 (12) and 4.1180 (08) Å, respectively (Table 1). Small shrinkage of unit cell constant and unit cell volume for the Eu^{3+} and Tb^{3+} ions suggested their substitution for Rb^+ -ion as their ionic sizes in higher

coordination are less than XII coordinated Rb^+ -ion [29]. The possible mechanism of charge compensation for a trivalent ion doped for divalent ions in mixed metal fluorides might be the generation of F^- interstitials causing asymmetry around the trivalent ion and disorder locally. These might also act as point defects in the lattice because of differences in the chemical valence and ionic radii among these ions [29].

UV-visible spectra of doped samples have been reproduced in Fig. 3. Bands at 265, 307, 371, 392, 415, and 523 nm, were noticed for $\text{RbZnF}_3:\text{Mn}^{2+}$ sample (Fig. 3(a)). The ground state configuration $(t_{2g})^3(e_g)^2$ of Mn^{2+} ($3d^5$) in cubic crystalline field have been found to result in ${}^6\text{A}_{1g}$, ${}^4\text{A}_{1g}$, ${}^4\text{E}_g$, ${}^4\text{T}_{2g}$, and ${}^4\text{A}_{2g}$ states along with other doublet states. Following this, observed absorbance could be attributed to the transitions from ${}^6\text{A}_{1g}$ (S) (ground state) to ${}^4\text{T}_{1g}$ (F), ${}^4\text{T}_{1g}$ (P), ${}^4\text{T}_{2g}$ (D), ${}^4\text{E}_g$ (D), ${}^4\text{A}_{1g}$ (G) and ${}^4\text{T}_{1g}$ (G) (excited states), respectively of Mn^{2+} -ion [30]. Bands signifying the transitions from $5d$ to $4f$ (${}^2\text{F}_{7/2}$ and ${}^2\text{F}_{5/2}$) of Ce^{3+} ion were present at 255 and 283 nm in addition to an intense band around 230 nm arising from ligand to metal charge transfer in the UV-visible spectrum of $\text{RbZnF}_3:\text{Ce}^{3+}$ sample (Fig. 3(b))[31]. In the UV-visible spectrum of $\text{RbZnF}_3:\text{Eu}^{3+}$ sample, transitions from the ground state of Eu^{3+} ion to its excited states of ${}^5\text{L}_6$, ${}^5\text{D}_2$ and ${}^5\text{D}_0$ appeared as bands at 397, 468 and 595 nm, respectively (Fig. 3(c)). Additionally, ligand-to-metal charge transfer (LMCT) bands in the UV region of the spectrum (234 and 272 nm) existed. Similarly, bands attributable to the transitions from ${}^7\text{F}_6$ (ground state) to ${}^5\text{D}_2$ and ${}^5\text{D}_3$ of Tb^{3+} (excited states) appeared at 331 and 373 nm, respectively for $\text{RbZnF}_3:\text{Tb}^{3+}$ sample (Fig. 3(d)).

Bands at 330, 351 and 394 nm arising possibly from the transitions of ${}^6\text{A}_{1g}$ (S) (ground state) to the ${}^4\text{E}_g$ (D), ${}^4\text{T}_{2g}$ (D), ${}^4\text{A}_{1g}$ (G), ${}^4\text{T}_{2g}$ (G) and ${}^4\text{T}_{1g}$ (G) (excited states) of octahedrally coordinated Mn^{2+} -ion, respectively were present in the photoluminescent excitation spectrum of

RbZnF₃:Mn²⁺ sample (Fig. 4(a)) [32]. Similarly, emission maxima occurring at 563 nm was attributed to ⁴T_{1g}(G) → ⁶A_{1g}(S) transition of Mn²⁺-ion. From the excitation and emission spectra of RbZnF₃:Ce³⁺ sample shown in Fig. 4(b), bands at 315 and 346 nm arising possibly from the parity-allowed transitions from the lowest 5*d* excited state to the spin-orbit component ²D of the doublet ground state, ²F_{5/2} and ²F_{7/2} of Ce³⁺-ion were noticed [33, 34]. In the excitation spectrum monitored at an emission wavelength of 320 nm, band at 246 nm assignable to the transition from 4*f* ground state of Ce³⁺ to the 5*d* excited state was observed. These features confirmed its presence in coordination environments higher than six. Luminescence emission in the red region at 593, 615, 650 and 698 nm were observed for Eu³⁺-doped sample (Fig. 4(c)). They corresponded to the ⁵D₀ → ⁷F_J (J = 1, 2, 3 and 4) transitions of Eu³⁺-ion, of which ⁵D₀ → ⁷F₁ and ⁵D₀ → ⁷F₃ transitions at 593 and 650 nm signified magnetic dipole transition and the rest were related to electric dipole transition. Their asymmetry ratio was found to depend strongly on the local symmetry of Eu³⁺ ions. The occupation of Eu³⁺ ions in octahedral sites, would introduce center of inversion for it. Under such conditions, intensity of magnetic dipole transition would be relatively strong, while the electric dipole transition would be very weak due to its partly forbidden nature. A strong electric dipole transition observed in the present case was an indication of electric field of low symmetry at the Eu³⁺ ions (C_{nv}, C_n and C_s) [35]. Moreover Judd-Oflet (J-O) intensity parameter (Ω_J) could provide additional information of covalent nature and local coordination of Eu³⁺-ion. The parameter Ω₂ and Ω₄ corresponding to the transition ⁵D₀-⁷F₂ and ⁵D₀-⁷F₄, respectively have been related directly to the emission intensity. Parameter, Ω₂ (3.06×10⁻²⁰ cm²) revealed about the existence of covalency and the structural changes in the local site symmetry of the Eu³⁺-ion (short range effect). Parameter, Ω₄, known to provide information about the long range effect, was estimated to be 9.83×10⁻²⁰ cm². The fact that Ω₂ was less than Ω₄

for the Eu-doped RbZnF₃ suggested a low degree of covalency for Eu³⁺ in the lattice [36-41]. The domination of ⁵D₀ → ⁷F₂ electric dipole transition at 615 nm over the ⁵D₀ → ⁷F₁ magnetic dipole transition at 593 nm led us to the conclusion that the Eu³⁺ ions were located in a disordered manner among the Rb⁺ sites in RbZnF₃ lattice explaining very well the absence of any inversion symmetry [29,36]. In the excitation spectrum monitored at an emission wavelength of 615 nm, bands at 360, 380 and 394 nm assignable to the ⁷F₀ (ground state) to ⁵D₄, ⁵G₂ and ⁵L₆ (excited state) transitions, respectively could be located. The observed bands at 315, 340, 350, 368 and 375 nm in the excitation spectrum of Tb³⁺ doped sample were assigned to transitions ⁷F₆ (ground state) to ⁵D₀, ⁵L₈, ⁵L₉, ⁵L₁₀ and ⁵G₆ (excited state) of Tb³⁺-ion, respectively (Fig. 4(d)). Emission bands in the green region at 468, 488, 545, 585 and 620 nm appeared for this sample which might be originating from ⁵D₃ → ⁷F₂, ⁵D₄ → ⁷F₆, ⁵D₄ → ⁷F₅, ⁵D₄ → ⁷F₄ and ⁵D₄ → ⁷F₃ transitions of Tb³⁺-ion [41, 43].

The emission decay curves for the doped samples have been presented in Fig. 5. While a bi-exponential behavior using the function $I = I_0 (\exp(-t/\tau_1) + \exp(-t/\tau_2))$ (I_0 is the initial emission intensity at $t = 0$) could be employed for a satisfactory fitting of the decay curves from Mn²⁺ and Ce³⁺ doped samples, single exponential behavior using the function $I = I_0 e^{-t/\tau}$ (where, I_0 is the initial emission intensity and τ is the emission lifetime) was found to be suffice for fitting of decay curves from Eu³⁺ and Tb³⁺ doped samples. From the fitting of decay of ⁴T_{1g} → ⁶A_{1g} (563 nm) transition of RbZnF₃:Mn²⁺ sample, decay times of 0.081 and 0.019 ms were estimated with a decay quantum efficiency of 74.5 and 25.5%, respectively (Fig. 5(a)). Similarly, decay times for RbZnF₃:Ce³⁺ were found to be 0.180 and 0.026 ms with decay efficiency of 79.25 and 20.25%, respectively (Fig. 5(b)). ⁵D₀ → ⁷F₂ (615 nm) transition of Eu³⁺-ion and ⁵D₄ → ⁷F₅ (545 nm) transition of Tb³⁺-ion decayed in 0.393 and 0.281 ms, respectively. The higher decay times could

be an over estimation. However, these times were considerably slower than decay time estimated for other doped fluoride host lattices investigated in the literature [44].

Conclusions

In summary, undoped and spectroscopically active ions doped haloperovskite RbZnF_3 were synthesized following a non-aqueous method. The cubic symmetry of the host lattice was preserved with dopants exercising their site preferences. The doped samples showed luminescence in blue, green and red regions and the time decay experiments suggested the uniform dispersion of them in the bulk samples. Of all the samples, strong green and red emission from Tb^{3+} and Eu^{3+} -doped samples, respectively with higher decay time suggested their use as efficient phosphor materials. These results will be beneficial to discover and optimize these systems for applications involving upconversion and other related optical phenomena.

Acknowledgement

Authors thank DST-SERB (EMR/2016/006131) Govt of India, for funding this research. SKS thanks UGC Govt of India for fellowship. Authors thank Prof. S. Uma for permitting to use her facilities funded by DST-SERB (EMR/2016/006762), Govt of India. Usage of facilities of CIF and M.Tech (NSNT) program of University of Delhi, Delhi are gratefully acknowledged.

References

- [1] C.N.R. Rao, B. Raveau, Transition metal oxides, VCH Publishers, Weinheim, Germany and New York, 1995.
- [2] A.S. Bhalla, R. Guo, R. Roy, The perovskite structure- a review of its role in ceramic science and technology, *Mater. Res. Innovations* 4 (2000) 3-26.
- [3] M.A. Pena, J.L. Fierro, Chemical structures and performance of perovskite oxides, *Chem. Rev.* 101 (2001) 1981-2018.
- [4] L.F. Johnson, H.J. Guggenheim, R.A. Thomas, Phonon-terminated optical masers, *Phys. Rev.* (1966) 179-186.
- [5] K.G. Belabaev, A. Kaminskii, S.E. Sarkisov, Stimulated emission from ferroelectric LiNbO₃ crystals containing Nd³⁺ and Mg²⁺ ions, *Phys. Status Solidi A* 28 (1975) K17-K20.
- [6] D. Dimos, C.H. Mueller, Perovskite thin films for high-frequency capacitor applications, *Annu. Rev. Mater. Sci.* 28 (1998) 397-419.
- [7] A. Huignard, T. Gacoin, J.P. Boilot, Synthesis and luminescence properties of colloidal YVO₄: Eu phosphors, *Chem. Mater.* 12 (2000) 1090-1094.
- [8] A. Braud, S. Girard, J.L. Doualan, M. Thuau, R. Mocorge, Energy-transfer processes in Yb: Tm doped KY₃F₁₀, LiYF₄ and BaY₂F₈ single crystals for laser operation at 1.5 and 2.3 μm, *Phys. Rev. B* 61 (2000) 5280-5292.
- [9] A. Kaminskii, *Laser Crystals*, 2nd Ed, Springer-Verlag, Berlin, 1990.
- [10] D.S. Crocket, H.M. Haendler, Synthesis of fluorometallates in methanol, some structure relationships, *J. Am. Chem. Soc.* 82 (1960) 4158-4162.

- [11] V. Kaiser, M. Otto, F. Binder, D. Babel, Jahn-Teller-Effekt und kristallstruktur-verzerrung bei den kupfer-fluorperowskiten NaCuF_3 und RbCuF_3 , Z. Anorg. Allg. Chem. 585 (1990) 93-104.
- [12] R.J. Arnott, J.M. Longo, The crystal structure of hexagonal RbNiF_3 (6H). J. Solid State Chem. 2 (1969) 416-420.
- [13] M.W. Shafer, T.R. McGuire, Preparation and properties of ferrimagnets in the RbMgF_3 - RbCoF_3 , J. Phys. Chem. Solids 30 (1968) 1989-1997.
- [14] J.C. Suits, T.R. McGuire, M.W. Shafer, Magnetic and optical properties of cobalt substituted RbNiF_3 , Appl. Phys. Lett. 12 (1968) 406-408.
- [15] J.A. Kafalas, J.M. Longo, Effect of pressure on the structure and magnetic properties of RbNiF_3 , Mater. Res. Bull. 3 (1968) 501-506.
- [16] H. Takeuchi, H. Ebisu, M. Arakawa, An electron paramagnetic resonance study of vanadium centres in RbZnF_3 single crystals, J. Phys. Condens. Matter 20 (2008) 055221 (7 pp).
- [17] Ph. Daniel, J. Toulouse, J.Y. Gesland, M. Rousseau, Raman-scattering investigation of the hexagonal perovskite RbZnF_3 , Phys. Rev. B 52 (1995) 9129-9132.
- [18] D.B. Mitzi, C.A. Field, W.T.A. Harrison, A.M. Guloy, Conducting tin halides with a layered organic-based perovskite structure, Nature 369 (1994) 467-469.
- [19] N.J. Jeon, J.H. Noh, W.S. Yang, Y.C. Kim, S. Ryu, J. Seo, S.II. Seok, Compositional engineering of perovskite materials for high-performance solar cells, Nature 517 (2015) 476-480.
- [20] S. Zhao, Y. Hou, X. Pei, Z. Xu, X. Xu, Upconversion luminescence of KZnF_3 : Er^{3+} , Yb^{3+} synthesized by hydrothermal method, J. Alloys Compd. 368 (2004) 298-303.
- [21] S. Ahmad, G. Vijaya Prakash, R. Nagarajan, Hexagonally ordered KLaF_4 host: phase-controlled synthesis and luminescence studies, Inorg. Chem. 51 (2012) 12748-12754.

- [22] J.H. Zeng, T. Xie, Z.H. Li, Y. Li, Monodispersed nanocrystalline fluoroperovskite up-conversion phosphors, *Cryst. Growth Des.* 7 (2007) 2774-2777.
- [23] S. Ahmad, R. Nagarajan, P. Raj, G. Vijaya Prakash, Novel fluorite structured superparamagnetic RbGdF₄ nanocrystals as versatile upconversion host, *Inorg. Chem.* 53 (2014) 10257-10265.
- [24] J. Grimm, O.S. Wenger, H.U. Gudel, Broadband green upconversion luminescence of Ni²⁺ in KZnF₃, *J. Lumin.* 102-103 (2003) 380-385.
- [25] L.K. Aminov, S.I. Nikitin, N.I. Silkin, A.A. Shakhov, R.V. Yusupov, Photoluminescence of KZnF₃: Ti⁺ and KMgF₃: Ti⁺ crystals, *J. Phys. Condens. Matter* 14 (2002) 13835-13856.
- [26] M.C. Marco de Lucas, F. Rodriguez, M. Moreno, Photoluminescence of RbCaF₃:Mn²⁺: The influence of phase transitions, *J. Phys. Condens. Matter* 5 (1993) 1437-1446.
- [27] N. Tyagi, P.S. Kumar, R. Nagarajan, Room temperature optical absorption and intrinsic photoluminescence in KZnF₃, *Chem. Phys. Lett.* 494 (2010) 284-286.
- [28] R. Roy, Multiple ion substitution in the perovskite lattice, *J. Am. Ceram. Soc.* 37 (1957) 581-588.
- [29] C.-Y. Lin, S.-H. Yang, J.-L. Lin, C.-F. Yang, Effects of the concentration of Eu³⁺ ions and synthesizing temperature on the luminescence properties of Sr_{2-x}Eu_xZnMoO₆ phosphors, *Appl. Sci.* 7 (2017) 30 (11 pp).
- [30] R. Kripal, H. Govind, M. Bajpai, M. Maurya, EPR and optical study of Mn²⁺ doped ammonium tartrate single crystals, *Spectrochim. Acta, Part A* 171 (2008) 1302-1306.
- [31] H.S. Jang, D.Y. Jeon, Yellow-emitting Sr₃SiO₅:Ce³⁺, Li⁺ phosphor for white-light-emitting diodes and yellow-light-emitting diodes, *Appl. Phys. Lett.* 90 (2007) 041906 (3 pp).

- [32] B. Henke, U. Rogulis, S. Schweizer, Optical and electron paramagnetic resonance studies on radiation defects in Mn-activated RbCdF₃, *Phys. Status Solidi C* 4 (2007) 1071-1074.
- [33] M. Yu, J. Lin, J. Fu, H.J. Zhang, Y.C. Han, Sol-gel synthesis and photoluminescent properties of LaPO₄:A (A = Eu³⁺, Ce³⁺, Tb³⁺) nanocrystalline thin film, *J. Mater. Chem.* 13 (2003) 1413-1419.
- [34] A.B. Shcherbakov, N.M. Zholobak, A.E. Baranchikov, A.V. Ryabova, V.K. Ivanov, Cerium fluoride nanoparticles protect cells against oxidative stress, *Mater. Sci. Eng. C* 50 (2015) 151-159.
- [35] X.Y. Chen, G.K. Liu, The standard and anomalous crystal-field spectra of Eu³⁺, *J. Solid State Chem.* 178 (2005) 419-428.
- [36] S.K. Gupta, M. Mohapatra, V. Natarajan, S.V. Godbole, Site-specific luminescence of Eu³⁺ in gel-combustion-derived strontium zirconate perovskite nanophosphors, *J. Mater. Sci.* 47 (2012) 3504-3515.
- [37] Ch.B. Annapurna Devi, Sk. Mahamuda, K. Swapna, M. Venkateswarlu, A. Srinivasa Rao, G. Vijaya Prakash, Compositional dependence of red luminescence from Eu³⁺ ions doped single and mixed alkali fluoro tungsten tellurite glasses, *Opt. Mater.* 73 (2017) 260-267.
- [38] H. Boubekri, M. Diaf, L. Guerbous, J.P. Jouart, Luminescence properties of Eu³⁺ doped CdF₂ single crystals, *Opt. Mater.* 78 (2018) 21-26.
- [39] Y.-S. Cho, Y.-D. Huh, Photoluminescence characteristics of green-emitting ZnGa₂S₄: Eu and EuGa₂S₄ phosphors, *Bull. Korean Chem. Soc.* 38 (2017) 493-498.
- [40] A.N. Yerpude, V.R. Panse, S.J. Dhoble, N.S. Kokode, M. Srinivas, Photoluminescence properties of Ca₂Al₂O₅:RE³⁺ (RE = Eu, Dy and Tb) phosphors for solid state lighting, *Luminescence* 32 (2017) 1361-1364.

- [41] B.V. Rao, G.V. Chalapathi, R.J. Kumar, Investigations on Eu^{3+} doped zinc phosphate glasses for photonic applications, *Int. J. Cur. Res. Rev.* 9 (2017) 19-24.
- [42] H. Boubekri, M. Diaf, K. Labbaci, L. Guerbous, T. Duvaut, J.P. Jouart, Synthesis and optical properties of Tb^{3+} doped CdF_2 single crystals, *J. Alloys Compd.* 575 (2013) 339-343.
- [43] B.D. Joshi, A.G. Page, Fluorescence and absorption spectra of Tb^{3+} ions in yttrium-gallium garnet, *J. Lumin.* 15 (1977) 29-34.
- [44] C.M. Combes, P. Dorenbos, C.W.E. Van Eijk, J.Y. Gesland, P.A. Rodnyi, Optical and scintillation properties of $\text{LiBaF}_3:\text{Ce}$ crystal, *J. Lumin.* 72-74 (1997) 753-755.

Figure Captions

Fig. 1 (a) Powder X-ray diffraction pattern, (b) EDX spectrum with analysis, (c) transmission electron microscopic image and (c) high resolution transmission electron microscopic image along with the selected area electron diffraction pattern of RbZnF_3 (in the inset).

Fig. 2 Rietveld refinement fitting of powder X-ray diffraction pattern of (a) RbZnF_3 and (b) manganese (II), (c) cerium (III), (d) europium (III) and (e) terbium (III) doped RbZnF_3 samples; red, experimental data; green line, calculated profile; pink line below, difference profile; vertical bars, Bragg position.

Fig. 3 UV-visible spectra of (a) manganese (II), (b) cerium (III), (c) europium (III) and (d) terbium (III) doped RbZnF_3 samples.

Fig. 4 Photoluminescence excitation and emission spectra of (a) manganese (II), (b) cerium (III), (c) europium (III) and (d) terbium (III) doped RbZnF_3 samples at room temperature. The excitation wavelength (λ_{ex}) and emission wavelength (λ_{em}) employed for obtaining the spectra are indicated in the respective plots.

Fig. 5 Photoluminescent emission life time (τ) decay curves of (a) manganese (II), (b) cerium (III), (c) europium (III) and (d) terbium (III) doped RbZnF_3 samples at room temperature.

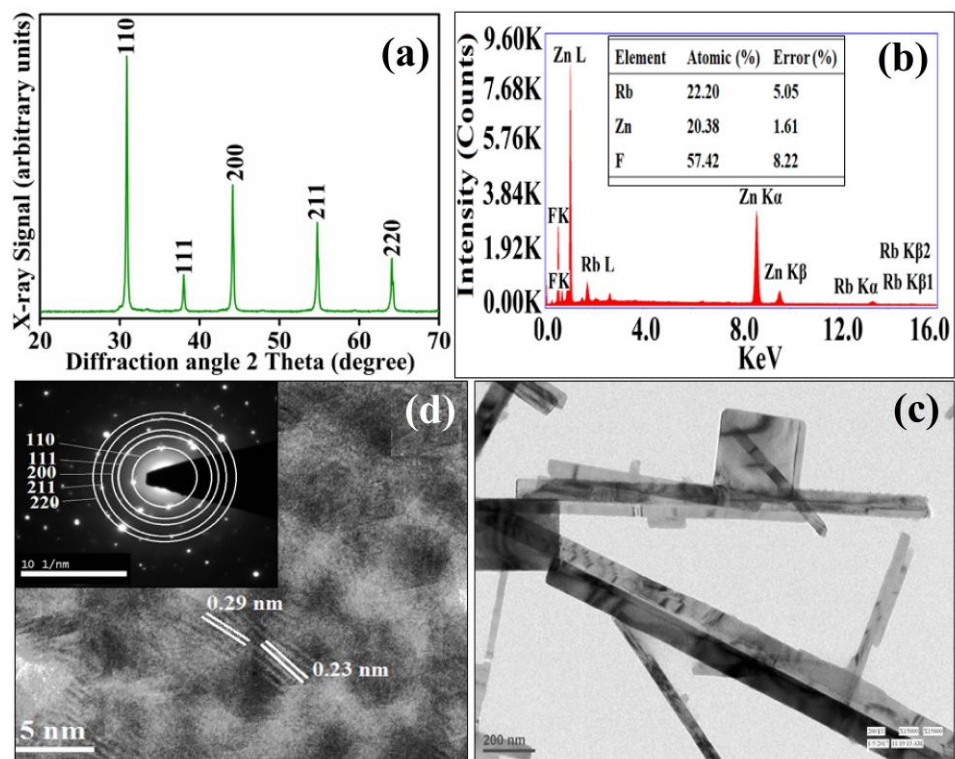


Fig. 1

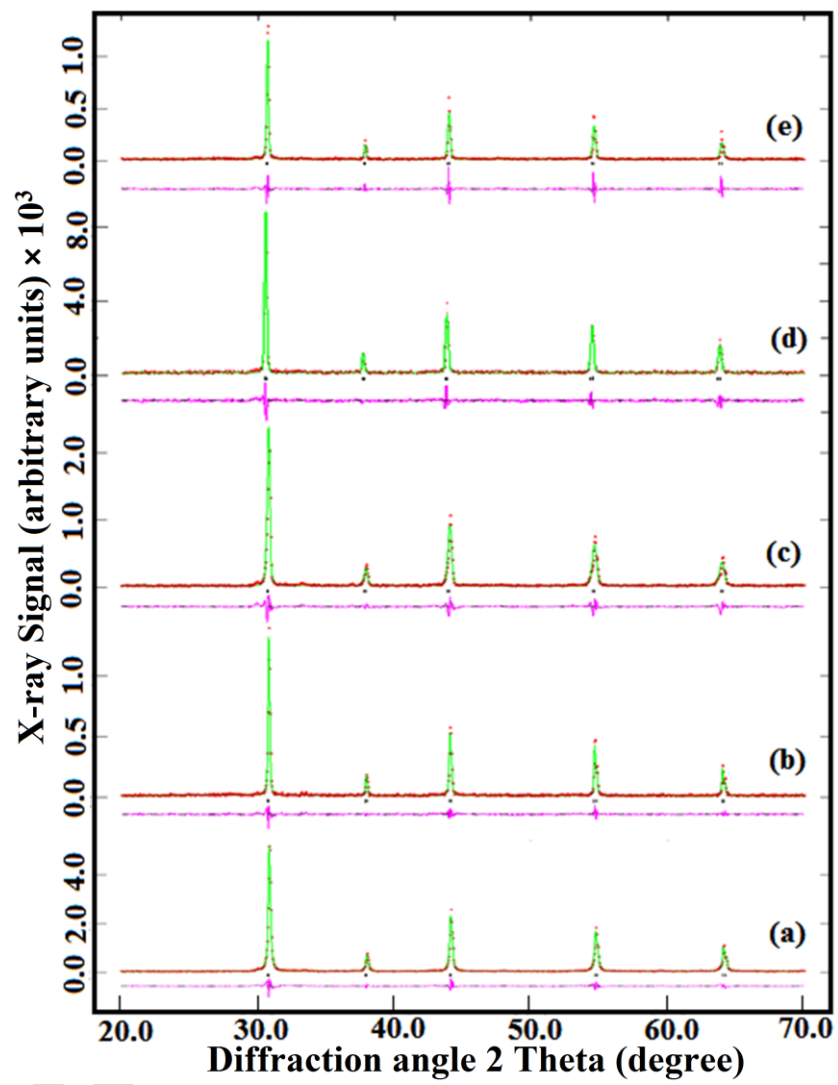


Fig. 2

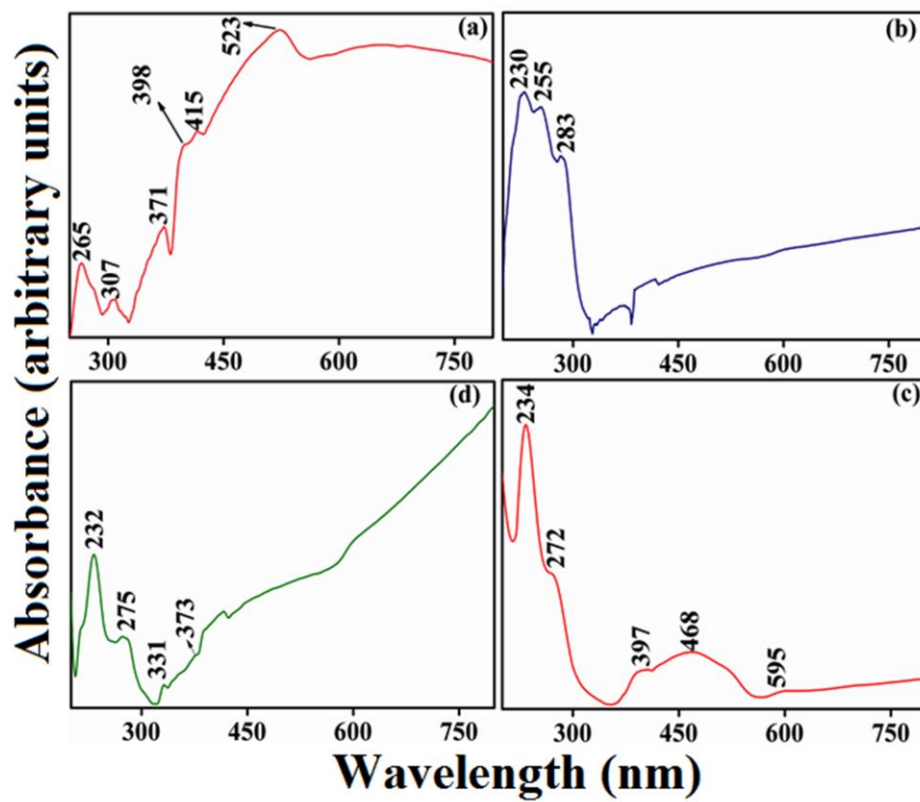


Fig. 3

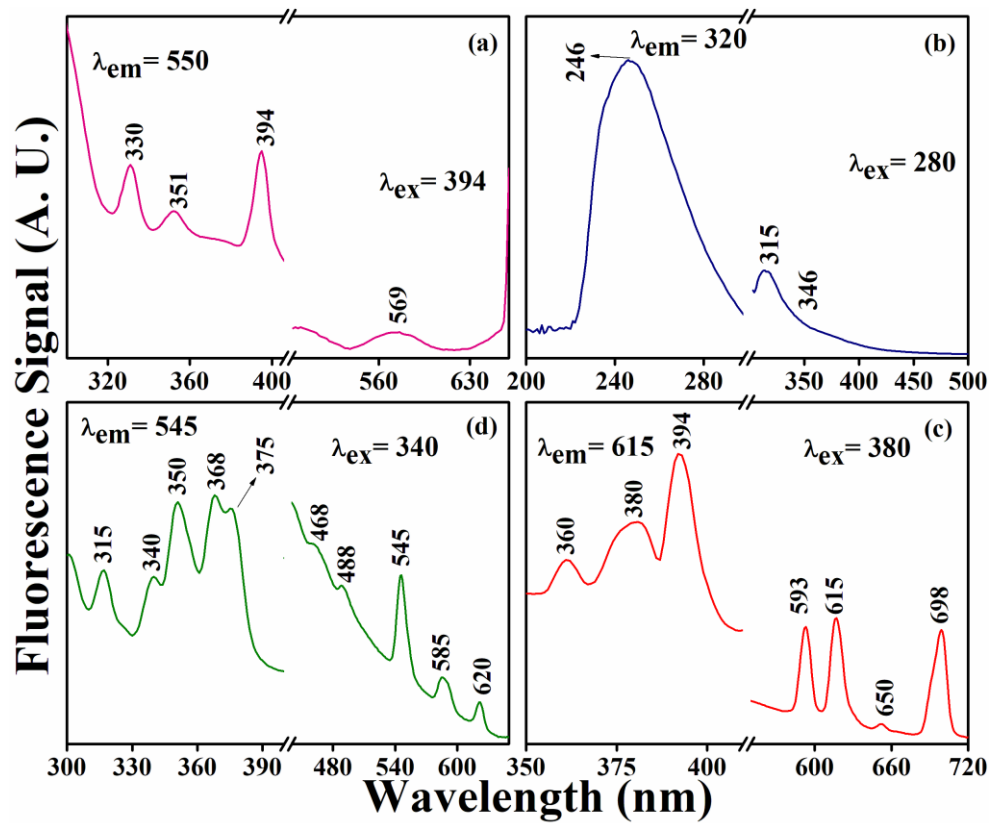


Fig. 4

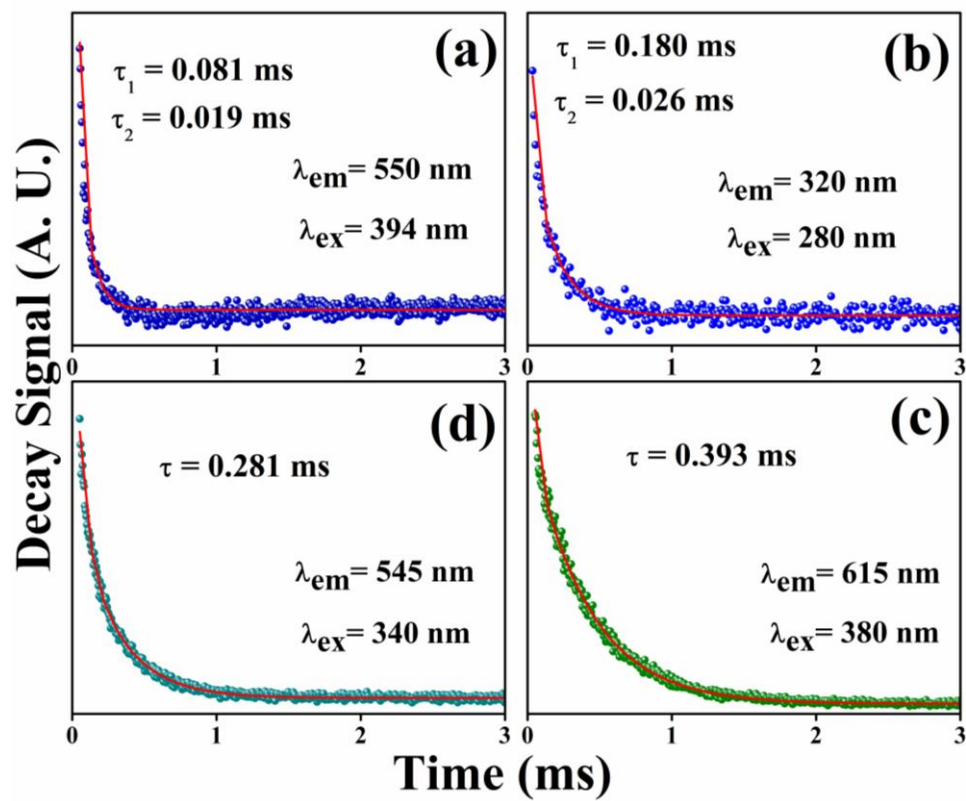


Fig. 5

Table 1 Summary of the crystallographic details from the Rietveld refinements of PXRD patterns undoped and doped RbZnF₃.

	RbZnF ₃	RbZnF ₃ :Mn ²⁺	RbZnF ₃ :Ce ³⁺	RbZnF ₃ :Eu ³⁺	RbZnF ₃ :Tb ³⁺
Crystal system	Cubic	Cubic	Cubic	Cubic	Cubic
Space group	<i>Pm</i> $\bar{3}$ <i>m</i>	<i>Pm</i> $\bar{3}$ <i>m</i>	<i>Pm</i> $\bar{3}$ <i>m</i>	<i>Pm</i> $\bar{3}$ <i>m</i>	<i>Pm</i> $\bar{3}$ <i>m</i>
<i>a</i> (Å)	4.1190 (16)	4.1238(28)	4.1180 (08)	4.1158 (12)	4.1141 (09)
Cell volume (Å ³)	69.255 (4)	70.699 (7)	69.836 (4)	69.722 (6)	69.636(5)
Formula weight (g/mol)	207.84	207.32	210.57	211.17	211.52
Z	1	1	1	1	1
ρ calc (g/cm ³)	4.9382	4.8692	5.0209	5.0290	5.0289
2 θ range	20-70°	20-70°	20-70°	20-70°	20-70°
No. of parameters	13	17	10	9	13
R _p (%)	0.1150	0.1889	0.1945	0.1823	0.1673
R _{wp} (%)	0.1505	0.2458	0.2519	0.2514	0.2224
χ^2	2.558	3.754	1.752	1.439	1.407

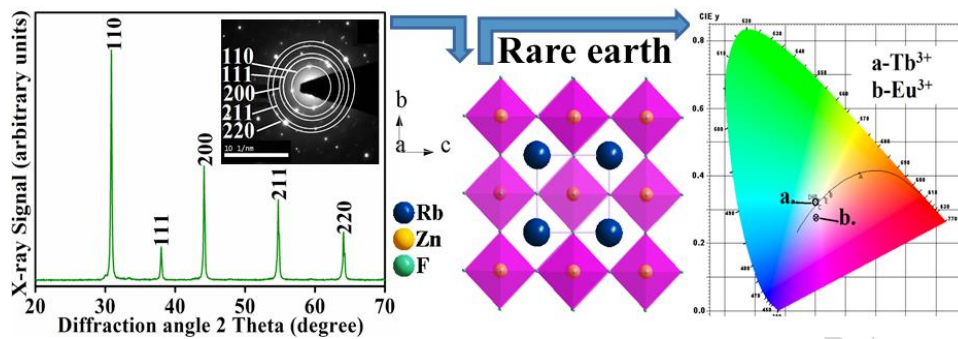
Table 2 Refined atomic parameters after the final cycle of refinement of RbZnF₃.

Atom	Site	S.O.F	<i>x</i>	<i>y</i>	<i>z</i>	U [Å ³]
Rb	<i>1a</i>	1	0.0	0.0	0.0	0.0250
Zn	<i>1b</i>	1	0.5	0.5	0.5	0.0250
F	<i>3c</i>	1	0.0	0.5	0.5	0.0250

Table 3 Refined atomic parameters after the final cycle of refinement for the rare-earth ion doped RbZnF₃.

Atom	Site	S.O.F	<i>x</i>	<i>y</i>	<i>z</i>	U [Å ³]
Rb	<i>1a</i>	0.95	0.0	0.0	0.0	0.0250
RE	<i>1a</i>	0.05	0.0	0.0	0.0	0.0250
Zn	<i>1b</i>	1.00	0.5	0.5	0.5	0.0250
F	<i>3c</i>	1.00	0.0	0.5	0.5	0.0250

TOC Graphic



Graphical abstract

ACCEPTED MANUSCRIPT

Highlights of the study

- Wet-chemical synthesis of cubic fluoroperovskite RbZnF_3
- Site selective doping at the Rb and Zn-sites
- Inverse perovskite arrangement for rare-earth ion doped samples.
- Luminescence in blue, green and red regions from doped samples with high decay time.

ACCEPTED MANUSCRIPT